Modifying Ru/C for Selective Hydrodeoxygenation of Carbohydrate-Rich Streams to Naphtha

Hannes Latine[a], Arthur Remans[a], Aleksei Turkin[a], Pierre Eloy[b], Damien P. Debecker[b], and Bert F. Sels*[a]

[a] Center for Sustainable Catalysis and Engineering (CSCE)
Katholieke Universiteit Leuven
Celestijnenlaan 200F, 3001 Heverlee, Belgium
E-mail: bert.sels@kuleuven.be; Phone number: +32 16 32 16 10

[b] Institute of Condensed Matter and Nanoscience (IMCN)
Université Catholique de Louvain
Place Louis Pasteur 1, 1348 Louvain-La-Neuve, Belgium

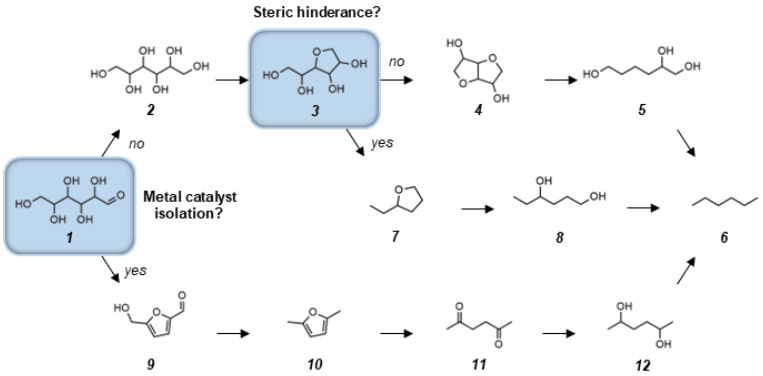
Abstract: Noble metals on carbon supports are promising catalysts for the hydrodeoxygenation of carbohydrate-rich waste streams into naphtha-range alkanes (C_5-C_9), key intermediates for fuels and chemicals. Among tested catalysts, Ru/C showed the highest activity due to its oxophilicity but suffered from excessive C-C cleavage, lowering C_6 alkane selectivity (39 C%). Pt/C achieved higher C_6 alkane selectivity (56 C%) by suppressing formation of intermediates prone to C-C scission, though its high cost limits scalability. To improve Ru/C performance, hydrothermal pretreatments with and without $H_4SiW_{12}O_{40}$ in solution were applied, boosting C_6 alkane yield to 56 C% and C_5-C_6 alkane yield to 66 C%, surpassing Pt/C catalysis. Ru dispersion remained intact at short residence times during pretreatment without $H_4SiW_{12}O_{40}$, while surface acidity was reduced, hindering C-O cleavage. The addition of $H_4SiW_{12}O_{40}$ during pretreatment restored acidity, incorporating reduced WOx species in the catalyst pores. However, excessive acid incorporation led to pore blockage and Ru oxidation to a less active RuO_2 phase. These findings emphasize the need to carefully balance acidity, metal oxidation state, particle size, and support porosity to optimize naphtha production from renewable carbohydrates.

Introduction

Addressing climate change without sacrificing prosperity demands a shift to sustainable chemical processes that replace essential products and precursors with renewable alternatives. Naphtha, a key feedstock for fuels, solvents, and polymer chemicals, is central to this transition. Sustainable naphtha production hinges on two factors: utilizing renewable resources and developing efficient catalysts.[1]

Transitioning away from a fossil-based linear economy is essential to reduce CO_2 emissions. Renewable feedstock – especially underutilized resources within the economy – should take priority, with fresh inputs used sparingly. Carbohydrates like cellulose and hemicellulose are particularly promising due to their abundance and versatility in sources such as agricultural residues, woody crops, furniture waste, and cardboard.[2] Besides, efficient catalysts are crucial for sustainable naphtha production, enabling reactions under milder conditions than conventional high-temperature, high-pressure processes. By lowering energy use, advanced catalysts can offer both environmental and economic benefits, supporting a more sustainable future.[3]

Current literature identifies two main pathways for converting cellulose to naphtha, with glucose as a key intermediate (Scheme 1). Both rely on acid-catalyzed steps (hydrolysis, dehydration) metal-catalyzed reactions (hydrogenation, hydrogenolysis), collectively known as hydrodeoxygenation (HDO). The sorbitol (SORB) pathway begins with glucose hydrogenation and proceeds via stable isosorbide intermediates, while the 5-hydroxymethylfurfural (HMF) pathway starts with glucose dehydration (or glucose isomerization followed by fructose dehydration) and proceeds through reactive furan intermediates.[4,5]



Scheme 1. Primary reaction pathways for cellulose hydrodeoxygenation, starting from glucose as key intermediate. 1: glucose, 2: sorbitol, 3: 1,4-sorbitan, 4: isosorbide, 5: 1,2,6-hexanetriol, 6: *n*-hexane, 7: 2-ethyltetrahydrofuran, 8:1,4-hexanediol, 9: 5-hydroxymethylfurfural, 10: 2,5-dimethylfuran, 11: 2,5-hexanedione, 12: 2,5-hexanediol.

Huber et al. first demonstrated the conversion of SORB to C_1-C_6 alkanes using Pt/SiO_2-Al_2O_3, achieving a 56 C% yield of *n*-hexane after 20 h.[6–9] Building on this, Tomishige et al. developed a system combining H_2SO_4 with Ir-ReOx/SiO_2, which enhanced C-O cleavage while suppressing C-C scission, resulting in a 95 C% *n*-hexane yield after 72 h.[10] They later applied this system to cellulose using H-ZSM-5 and Ir-ReOx/SiO_2, achieving 83 C% *n*-hexane in 12 h.[4] Sels et al. initially used $H_4SiW_{12}O_{40}$ and Ru/C to convert cellulose to hexitols, later shifting to a faster route via glucose dehydration, achieving 75 C% C_5-C_6 alkanes in 6 h.[5,11] Inspired by Buntara et al.'s findings on the higher reactivity of HMF over isosorbide, they prioritized glucose dehydration to avoid stable intermediates.[12] Ma and Zhang further explored the SORB route using H_3PO_4 and Ru/C, introducing $LiNbMoO_6$ to suppress isosorbide formation and promote 1,4-sorbitan ring opening to 2-ethyltetrahydrofuran, achieving 78 C% C_5-C_6 alkanes after 24 h.[13] They later streamlined the system by replacing ReOx with WOx in the Ir-ReOx/SiO_2 catalyst, reaching 93 C% C_5-C_6 alkane yield after 24 h.[14]

Among catalytic systems for cellulose conversion, the HMF pathway has shown greater efficiency in producing naphtha. However, achieving selective conversion still requires critical modifications to minimize side reactions and improve yield. A promising approach involves a biphasic reaction medium with an aqueous liquid phase containing hydrophilic $H_4SiW_{12}O_{40}$ and an organic liquid phase with hydrophobic Ru/C. This setup prevents glucose hydrogenation and HMF condensation by isolating the catalysts. Enhancing Ru/C catalyst performance further can be achieved by reducing RuOx to Ru^0, boosting hydrogenation activity. Controlled Ru particle sintering promotes planar HMF adsorption over point adsorption of glucose, reducing glucose hydrogenation. Additionally, incorporating $H_4SiW_{12}O_{40}$ into Ru/C pores facilitates efficient cycling between dehydration and hydrogenation, promoting selective C-O cleavage over C-C scission, thereby improving carbon efficiency towards naphtha alkanes. These catalytic enhancements are attributed to hydrothermal pretreatment (HTP) in acidic media.[5]

Catalytic HDO shares conceptual similarities with conventional hydrotreating reactions such as hydrodesulfurization and hydrodenitrogenation, which typically use sulfided $CoMo/Al_2O_3$ or $NiMo/Al_2O_3$ catalysts. However, the oxygenated nature of carbohydrate feedstocks causes rapid sulfur loss and deactivation of these materials, limiting their direct applicability to HDO.[15,16] Consequently, sulfur-free variants, such as CoMoOx and NiMoOx alloys, or their carbide and phosphide analogues, have been developed to bridge the gap between hydrotreating and HDO catalysis. These materials can activate hydrogen and cleave C-O bonds without relying on sulfur, yet they often exhibit lower hydrogenation activity or require higher temperatures than noble metals.[17,18] Therefore, Ru/C, Pd/C, and Pt/C are frequently used instead, as they remain active and stable under aqueous, sulfur-free conditions and effectively promote oxygen removal from biomass-derived molecules.

The mechanisms by which HTP alters Ru/C catalyst properties are not well understood, and a systematic investigation of the physicochemical changes in Ru/C after HTP is lacking. Additionally, the potential of other noble metal catalysts, such as Pd/C and Pt/C, under similar conditions has been less explored. This study aims to fill these gaps by systematically investigating Ru/C, Pd/C, and Pt/C catalysts synthesized under varying HTP conditions, with the goal of identifying key catalyst features that drive selective HDO of carbohydrate-rich streams.

Results and Discussion

Rationale

To investigate the rationale for using Ru/C in the selective production of naphtha-type alkanes via the HMF pathway, commercially available, unpretreated 5 wt% Ru/C, Pd/C, and Pt/C catalysts from Sigma-Aldrich were tested under identical conditions (Figure 1).

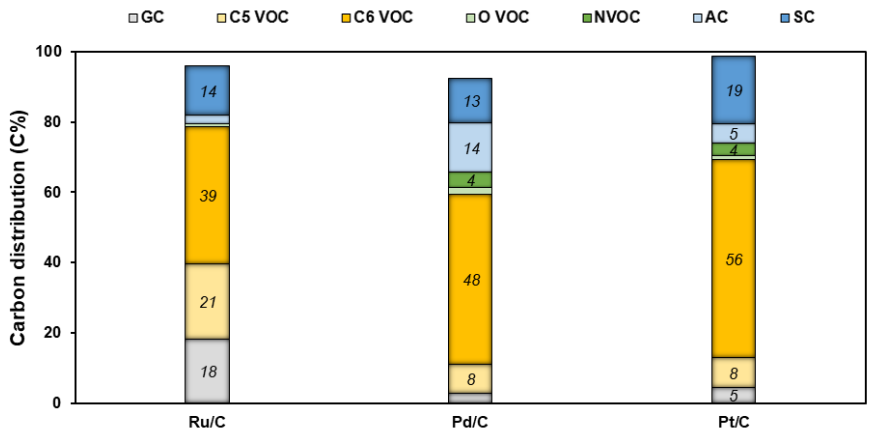
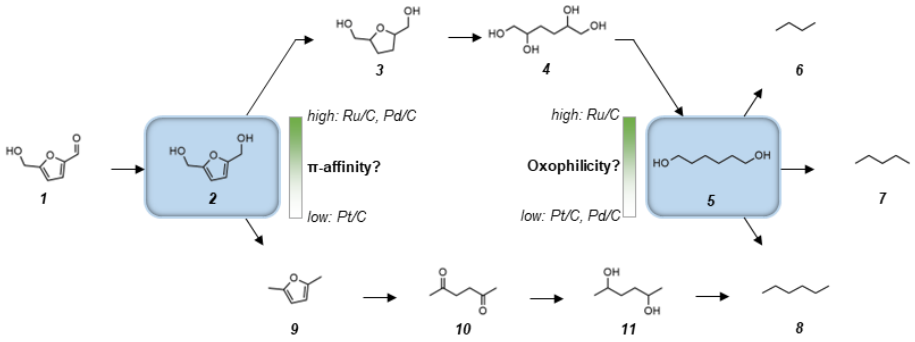


Figure 1. Carbohydrate hydrodeoxygenation over unmodified metal catalysts: influence of noble metal element on carbon distribution. Gaseous carbon (GC): $<C_5$ alkanes. Volatile organic carbon (VOC): C_5 alkanes (C5 VOC), C_6 alkanes (C6 VOC), and alcohols and cyclic ethers (O VOC). Non-volatile organic carbon (NVOC): $C_6<$ alkanes, benzenes, phenolics. Aqueous carbon (AC): monosaccharides, (poly)alcohols, cyclic ethers. Solid carbon (SC): highly condensed brownish residue, closely related to char(coal). Standard HTP conditions: 1.0 g metal catalyst, 0 mM $H_4SiW_{12}O_{40}$, 40 mL H_2O, 600 rpm, 50 bar H_2, 20-210 °C (10 °C/min), 60 min at final temperature. Standard HDO conditions: 2.0 g birch pulp (85 C% cellulose, 9 C% hemicellulose, 6 C% lignin), 50 mM $H_4SiW_{12}O_{40}$, 0.50 g metal catalyst, 30 mL H_2O, 9.5 mL cyclohexane, 0.5 mL n-heptane, 900 rpm, 50 bar H_2, 20-280 °C (12 °C/min), 60 min at final temperature. The typical experimental error in gaseous carbon (±1.2%), volatile organic carbon (±1.5%), non-volatile organic carbon (±0.6%), aqueous carbon (±0.3%), and solid carbon (±1.3%) was determined from triplicate measurements of a representative reaction.

Among the catalysts tested, Ru/C achieved the highest overall C_1-C_6 alkane yield (79 C%), while Pt/C showed the highest selectivity for C_6 alkanes (56 C%). The superior alkane yield of Ru is mainly due to its high intrinsic hydrogenation activity, efficiently dissociating molecular hydrogen and generating a high local concentration of active hydrogen species, promoting complete hydrogenation and deoxygenation. In contrast, Pd and Pt exhibit different catalytic behaviors. Pd favors partial hydrogenation and selective reduction of unsaturated bonds, often retaining oxygen functionalities, which results in higher yields of aqueous carbon and non-volatile organic carbon (2 vs. 12 C%, 0 vs. 4 C%, respectively). Pt, known for stabilizing aromatic structures, shows limited activity towards complete hydrogenation, leading to increased formation of both solid and aqueous carbon (14 vs. 19 C%, 2 vs. 5 C%, respectively) due to the polymerization of accumulated furanic intermediates.[19]

Differences in C_6 alkane yield are primarily influenced by the metal's π-affinity and oxophilicity (Scheme 2). Pt interacts weakly with aromatic rings, often in a tilted geometry, limiting full hydrogenation and preserving aromaticity, which favors the formation of 2,5-dimethylfuran (DMF) over 2,5-di(hydroxymethyl)tetrahydrofuran (DHTHF). In contrast, Ru and Pd adsorb aromatic rings flatly, enhancing π-interactions and facilitating complete stepwise hydrogenation.[20] Ru, owing to its higher oxophilicity compared to Pd and Pt, interacts strongly with oxygenated species, facilitating efficient C-O bond cleavage along the DHTHF pathway to yield *n*-hexane. However, under the applied conditions, Ru also activates C-C bonds adjacent to oxygen atoms, leading to the formation of lighter alkanes such as *n*-pentane, *n*-butane, and CH_4.[5,21] Pd and Pt, with lower oxophilicity, tend to favor selective C=C or C-O bond cleavage, preserving the C-C framework and limiting fragmentation into lighter C_1-C_5 alkanes, instead selectively producing C_6 alkanes. Thus, Pd mainly forms 1-hexanol and *n*-hexane via the DHTHF pathway, while Pt selectively produces *n*-hexane through the DMF pathway.



Scheme 2. Primary reaction pathways for 5-hydroxymethylfurfural hydrodeoxygenation. 1: 5-hydroxymethylfurfural, 2: 2,5-di(hydroxymethyl)furan, 3: 2,5-di(hydroxymethyl)tetrahydrofuran, 4: 1,2,5,6-hexanetetraol, 5: 1,6-hexanediol, 6: *n*-butane, 7: *n*-pentane, 8: *n*-hexane, 9: 2,5-dimethylfuran, 10: 2,5-hexanedione, 11: 2,5-hexanediol.

Pt's scarcity and high cost limit its practical use, making a more sustainable strategy desirable. A promising approach is to modify the more abundant and cost-effective Ru catalyst to achieve Pt-like C_6 selectivity, combining Ru's high activity with Pt's selectivity. Inspired by previous work, this selectivity shift can be achieved via HTP in acidic aqueous media.[5] HTP modifies the Ru/C catalyst in several ways: under a H_2 atmosphere, RuOx species are reduced to catalytically active Ru^0, improving hydrogenation efficiency. Simultaneously, heating in H_2O causes Ru particles to cluster, creating smoother surfaces that suppress adsorption of glucose. This prevents glucose from hydrogenating into SORB, which converts less efficiently to *n*-hexane than HMF. By promoting planar adsorption and ring hydrogenation of aromatics like HMF, Ru sintering steers the reaction toward deoxygenation. To further favor deoxygenation along the DMF pathway over the DHTHF pathway, acidity near the Ru sites is enhanced by

adding an acid catalyst, $H_4SiW_{12}O_{40}$, to the aqueous phase. This heteropoly acid, which has a strong affinity for the carbon support, penetrates the pores and deposits near Ru particles, facilitating synergistic dehydration-hydrogenation reactions. Even if 1,2,5,6-hexanetetraol forms, the acid promotes C-O bond cleavage over C-C scission, improving carbon retention in the final alkane product. To disentangle the respective roles of metal particle modification and acid incorporation while identifying the most optimal HTP conditions, both residence time and $H_4SiW_{12}O_{40}$ concentration were systematically varied.

Hydrothermal Pretreatment Residence Time

To examine the impact of Ru oxidation state on C_6 alkane yield, XPS analysis was conducted on Ru/C catalysts subjected to HTP without $H_4SiW_{12}O_{40}$ and varying residence times (Figure 2, Table 1, Figure S1). Our results show a progressive decrease in Ru oxidation state with increasing residence time, with Ru^0/RuOx ratios rising from 0.08 (no HTP) to 0.18 (180 min, 0 mM). During HTP, prolonged exposure to a reducing H_2 atmosphere at elevated temperature gradually converts surface RuOx into Ru^0. H_2, being a strong reductant at these temperatures, stepwise removes lattice oxygen and promotes restructuring towards more reduced surface species.[5] Because this reduction is time-dependent, longer residence times allow more complete removal of surface oxide, resulting in higher Ru^0/RuOx ratios. In principle, an increase in Ru^0 should enhance catalytic activity, as Ru^0 is generally more effective at activating H_2 than its oxidized RuOx counterparts.[22,23] However, the highest C_6 alkane yields were obtained at shorter residence times (30 and 60 min, 0 mM), suggesting that factors other than the Ru^0/RuOx ratio may counteract the expected benefits of further reduction. Compared to the unpretreated Ru/C catalyst, the C_6 alkane yield slightly increased (39 vs. 45 C%), while C_5 and C_1-C_4 alkane yields slightly decreased (21 vs. 19 C%, 19 vs. 16 C%, respectively).

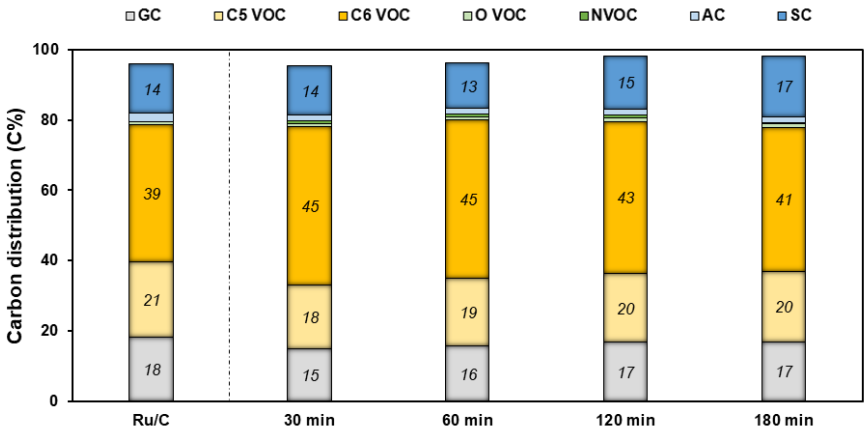


Figure 2. Carbohydrate hydrodeoxygenation over modified Ru/C catalysts: influence of hydrothermal pretreatment residence time on carbon distribution. Gaseous carbon (GC): <C_5 alkanes. Volatile organic carbon (VOC): C_5 alkanes (C5 VOC), C_6 alkanes (C6 VOC), and alcohols and cyclic ethers (O VOC). Non-volatile organic carbon (NVOC): C_6< alkanes, benzenes, phenolics. Aqueous carbon (AC): monosaccharides, (poly)alcohols, cyclic ethers. Solid carbon (SC): highly condensed brownish residue, closely related to char(coal). Standard HTP conditions: 1.0 g metal catalyst, 0 mM $H_4SiW_{12}O_{40}$, 40 mL H_2O, 600 rpm, 50 bar H_2, 20-210 °C (10 °C/min), 60 min at final temperature. Standard HDO conditions: 2.0 g birch pulp (85 C% cellulose, 9 C% hemicellulose, 6 C% lignin), 50 mM $H_4SiW_{12}O_{40}$, 0.50 g metal catalyst, 30 mL H_2O, 9.5 mL cyclohexane, 0.5 mL n-heptane, 900 rpm, 50 bar H_2, 20-280 °C (12 °C/min), 60 min at final temperature. The typical experimental error in gaseous carbon (±1.2%), volatile organic carbon (±1.5%), non-volatile organic carbon (±0.6%), aqueous carbon (±0.3%), and solid carbon (±1.3%) was determined from triplicate measurements of a representative reaction.

To further characterize the Ru species and complement the XPS findings, TPR was used to monitor H_2 consumption across specific temperature ranges, providing insights into the oxidation states of Ru species (Figure S2). According to the literature, Ru/C catalysts typically show two major H_2 consumption peaks: one around 120 °C, associated with the reduction of highly oxidized RuOx (x > 2) to Ru^{2+}, and another near 240 °C, corresponding to the reduction of Ru^{2+} to Ru^0.[24–28] In the unpretreated Ru/C catalyst, both peaks are present, with the Ru^{2+} peak being more intense. In contrast, the 180 min pretreated Ru/C catalyst also shows both peaks, but the RuOx peak is more prominent. These results confirm that the Ru^0/RuOx ratio increases with residence time and that Ru^{2+} is formed more easily than the highly oxidized RuOx forms (x > 2) during HTP. To further verify the presence and structure of different Ru species, XRD analysis was performed (Figure S3a). Ru^0 exhibits characteristic reflections at 38.6° (100), 42.4° (002), 44.4° (101), and 58.8° (102), corresponding to hexagonal close-packed Ru (JCPDS 00-001-1253).[29,30] Among these, the 44.4° reflection is the most intense and was observed in all Ru/C catalysts. However, reflections corresponding to crystalline RuO_2 at 28.0°, 35.0°, 40.2°, 54.2°, 57.9°, and 59.4° (JCPDS 00-040-1290) were not detected.[31] This suggests that higher oxidation states of RuOx (x ≥ 2), which are typically amorphous or metastable, dominate in the Ru/C catalysts and are difficult to detect by XRD.[32,33]

Table 1. XPS results of hydrothermally pretreated Ru/C catalysts.

Entry	Pretreatment		Elemental composition							
	Time (min)	Acid (mM)	Ru^0 (%)	RuOx (%)	Ru^0/RuOx (-)	COOH (%)	CO (%)	COH (%)	O (%)	W (%)
1	0	0	0.08	1.05	0.08	3.49	3.56	2.92	9.02	0.00
2	30	0	0.13	1.02	0.12	2.86	3.01	2.94	8.32	0.00
3	60	0	0.14	0.96	0.15	3.31	2.10	1.16	8.32	0.00
4	120	0	0.11	0.99	0.11	2.89	2.74	3.09	8.38	0.00
5	180	0	0.18	0.90	0.20	3.28	0.01	0.00	6.85	0.00
6	60	2	0.08	0.94	0.09	2.78	2.50	2.71	6.85	0.18
7	60	4	0.08	1.00	0.08	2.78	2.69	2.59	10.5	0.62
8	60	50	0.04	0.93	0.04	2.57	2.46	1.88	16.5	1.57
9	60	100	0.03	0.74	0.04	3.03	3.00	3.40	10.5	1.68

Although the amount of Ru^0 increases with residence time, it is important to note that the highest C_6 alkane yield is not achieved at the highest Ru^0 content, but rather at shorter residence times (30 and 60 min, 0 mM). This suggests that Ru^0 content alone does not determine alkane yield. Another critical factor is the Ru dispersion and particle size, as these influence both catalytic activity and selectivity. To assess Ru dispersion and particle size, CO chemisorption measurements were conducted, assuming spherical particles and a uniform distribution of the

three main low-index facets – (111), (100), and (110) – on the Ru surface (Table S2).[34] The results show that Ru particle size increases with residence time, from 5.3 nm (no HTP) to 11 nm (180 min, 0 mM). This increase reflects Ru sintering, which reduces the number of accessible Ru sites, thereby suppressing glucose hydrogenation and decreasing overall catalytic activity.[5] The highest C_6 alkane yield was obtained with an intermediate Ru particle size (~6 nm), slightly larger than that of the unpretreated catalyst. Given that this size is several times larger than the molecular diameter of HMF (~1 nm) (Figure S4), particle curvature – rather than size itself – may be the primary factor influencing C_6 alkane selectivity. This interpretation is consistent with reports showing that curvature and coordination environment, rather than particle diameter alone, influence adsorption geometry and C-O bond scission pathways on Ru and related metals. Highly curved surfaces expose many undercoordinated Ru atoms, which promote strong adsorption and deep hydrogenation, often suppressing selective C-O cleavage, while flatter surfaces stabilize adsorption modes that more readily undergo C-O bond scission.[35,36] However, excessive sintering clearly reduces total alkane yield by lowering the number of active sites.

Furthermore, the rise in C_1-C_5 alkane formation at prolonged residence times (33 vs. 37 C%) suggests that also other factors may contribute. Reducing conditions during HTP could not only influence Ru oxidation states but also alter the surface chemistry of the carbon support. To verify this hypothesis, NH_3-TPD was performed to assess the acidic properties of the Ru/C catalyst (Figure 3, Table S3). Literature suggests that carbon-based catalysts with adsorbed heteropoly acids display a range of acidic behaviors.[37–39] Weak acid sites are typically observed through desorption signals between 150 °C and 300 °C, often appearing as split peaks near 260 °C and 280 °C, which are primarily attributed to phenol and carbonyl functionalities on the carbon support. Moderate acid sites desorb NH_3 between 300 °C and 450 °C, usually associated with carboxyl groups, and their signals tend to be less pronounced than those of the weak acidic sites.

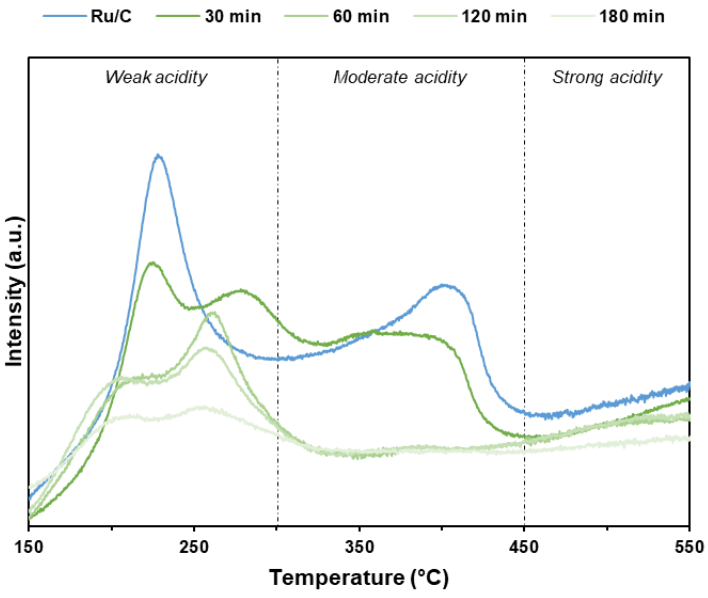


Figure 3. NH_3-TPD results of hydrothermally pretreated metal catalysts without $H_4SiW_{12}O_{40}$.

In agreement with XPS results, carbonyl and alcohol functionalities are nearly completely reduced, consistent with the hydrogen spillover effect, where activated hydrogen atoms generated at Ru sites migrate to adjacent carbon functional groups, leading to their reduction (Table 1, Figure S1). Although XPS shows that the amount of carbon associated with carboxylic groups remains nearly constant, the NH_3-TPD results indicate a strong decrease in moderate acidity. This can be explained by a loss of protonic activity rather than chemical removal: carboxylic

groups may still be present but converted into less acidic forms (e.g. carboxylates or hydrogen-bonded species) or become less accessible for NH_3 adsorption. As a result, their chemical signature remains visible in XPS, while their functional acidity decreases. These findings suggest that, alongside Ru sintering, the loss of surface oxygen groups may also contribute to the reduced C_6 selectivity and increased fragmentation at prolonged HTP conditions.

Hydrothermal Pretreatment $H_4SiW_{12}O_{40}$ Concentration

To assess the impact of acid incorporation in the pores of the Ru/C catalyst on C_6 alkane yield, XPS was performed on Ru/C catalysts subjected to HTP with varying $H_4SiW_{12}O_{40}$ concentrations (Figure 4, Table 1, Figure S1). The results show a clear trend of increasing acid incorporation with higher $H_4SiW_{12}O_{40}$ concentrations, as indicated by the rising W content from 0.0% (no HTP) to 1.7% (60 min, 100 mM), respectively. This trend is supported by TGA data, which shows the weight fraction of acid incorporation in Ru/C increasing from 0% (no HTP) to 24% (60 min, 100 mM) (Table S4).

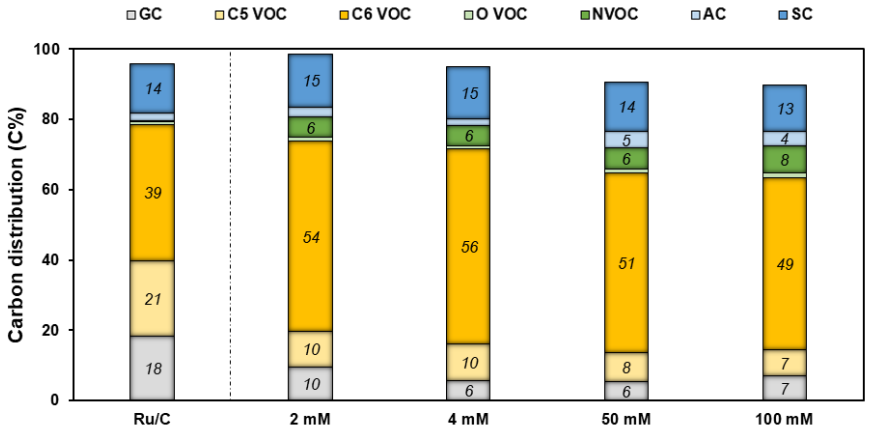


Figure 4. Carbohydrate hydrodeoxygenation over modified Ru/C catalysts: influence of hydrothermal pretreatment $H_4SiW_{12}O_{40}$ concentration on carbon distribution. Gaseous carbon (GC): $<C_5$ alkanes. Volatile organic carbon (VOC): C_5 alkanes (C5 VOC), C_6 alkanes (C6 VOC), and alcohols and cyclic ethers (O VOC). Non-volatile organic carbon (NVOC): $C_6<$ alkanes, benzenes, phenolics. Aqueous carbon (AC): monosaccharides, (poly)alcohols, cyclic ethers. Solid carbon (SC): highly condensed brownish residue, closely related to char(coal). Standard HTP conditions: 1.0 g metal catalyst, 0 mM $H_4SiW_{12}O_{40}$, 40 mL H_2O, 600 rpm, 50 bar H_2, 20-210 °C (10 °C/min), 60 min at final temperature. Standard HDO conditions: 2.0 g birch pulp (85 C% cellulose, 9 C% hemicellulose, 6 C% lignin), 50 mM $H_4SiW_{12}O_{40}$, 0.50 g metal catalyst, 30 mL H_2O, 9.5 mL cyclohexane, 0.5 mL n-heptane, 900 rpm, 50 bar H_2, 20-280 °C (12 °C/min), 60 min at final temperature. The typical experimental error in gaseous carbon (±1.2%), volatile organic carbon (±1.5%), non-volatile organic carbon (±0.6%), aqueous carbon (±0.3%), and solid carbon (±1.3%) was determined from triplicate measurements of a representative reaction.

Despite the progressive acid loading, the highest C_6 alkane yields were observed for the Ru/C catalyst pretreated with 4 mM $H_4SiW_{12}O_{40}$. Compared to the unpretreated Ru/C catalyst, the C_6 alkane yield substantially increased (39 vs. 56 C%), while C_5 and C_1-C_4 alkane yields decreased (21 vs. 10 C%, 19 vs. 6 C%, respectively). Notably, acid incorporation not only promotes C-O over C-C cleavage but also facilitates C-C coupling through condensation and alkylation of furanic intermediates within the Ru/C catalyst pores, as evidenced by the formation of non-volatile organic carbon (0 vs. 6 C%) upon acid incorporation. GC analysis of this fraction revealed the presence of *n*-decane and *n*-dodecane, likely resulting from HDO of FA self-alkylation and HMF self-condensation products, respectively.[40,41]

To characterize the incorporated acidity, NH_3-TPD was performed to assess the strength of the acid sites on the Ru/C catalyst (Figure S5). Ru/C catalysts pretreated with low $H_4SiW_{12}O_{40}$ concentrations (60 min, 2 and 4 mM) show a marked reduction in weak and moderate acidity compared to the unpretreated catalyst, likely due to the loss of surface carboxyl, carbonyl, and alcohol groups under the reducing H_2 atmosphere. In contrast, catalysts treated with higher $H_4SiW_{12}O_{40}$ concentrations (60 min, 50 and 100 mM) show a gradual recovery in weak and moderate acidity relative to the low-acid samples. Strong acidic sites, such as those from the Keggin-structured $H_4SiW_{12}O_{40}$, exhibit desorption behavior around 525 °C.[37–39] However, no desorption signals characteristic of strong acidity were detected in any sample, suggesting that $H_4SiW_{12}O_{40}$ is also reduced under H_2-rich HTP conditions, preventing the incorporation of its intact Keggin structure.[37–39]

To clarify the nature of the incorporated acid, XRD analysis was performed to determine whether $H_4SiW_{12}O_{40}$ is present in its bulk Keggin structure within the Ru/C catalyst (Figure S3b). The characteristic reflections of the Keggin structure are reported at 17.9°, 20.6°, 25.2°, 29.2°, 34.5°, 37.7°, and 52.9°, with the 25.2° peak typically being the most intense (JCPDS 00-001-0559).[42] However, none of these reflections were detected in the diffractograms of Ru/C catalysts, regardless of the $H_4SiW_{12}O_{40}$ concentration used during HTP. This absence suggests that $H_4SiW_{12}O_{40}$ is not incorporated in its bulk Keggin form, consistent with NH_3-TPD results indicating partial decomposition or high dispersion of the acid phase (Figure S5). These findings align with previous studies showing that $H_4SiW_{12}O_{40}$ does not crystallize upon incorporation and instead likely forms dispersed WOx species.[43,44]

This hypothesis is further supported by H_2-TPR analysis, which shows WO_3-related reduction peaks around 600 °C (Figure 5). The peak area increases progressively with higher $H_4SiW_{12}O_{40}$ pretreatment concentrations, indicating gradual WO_3 formation. This trend aligns with NH_3-TPD data, reinforcing the idea that WO_3 contributes to the observed weak and moderate acidity (Figure S5). This added acidity likely plays a key role in the improved performance of $H_4SiW_{12}O_{40}$-pretreated Ru/C catalysts. The catalytic role of WO_3 is consistent with findings by Ma and Zhang, who demonstrated its effectiveness as a modifier for enhancing hydrogenolysis activity.[14] These results highlight the importance of WO_3 species on the catalyst surface in promoting selective transformations during HDO reactions.

The color variations of WOx species, which reflect their oxidation state, offer further insight into the chemical transformations during HTP. After pretreatment, the acid solution appeared dark blue – characteristic of tungsten blue oxide, a poorly defined mixture typically containing WO_3, WO_2, and other reduced WOx species.[45] When exposed to air at room temperature, the solution gradually turned green, indicating oxidation of the reduced WOx species back to yellowish WO_3 (Figure S6). These visual changes support the hypothesis that $H_4SiW_{12}O_{40}$ is partially or fully reduced under H_2-rich HTP conditions, leading to decomposition of the Keggin structure and the formation of lower WOx species such as WO_3 and WO_2.

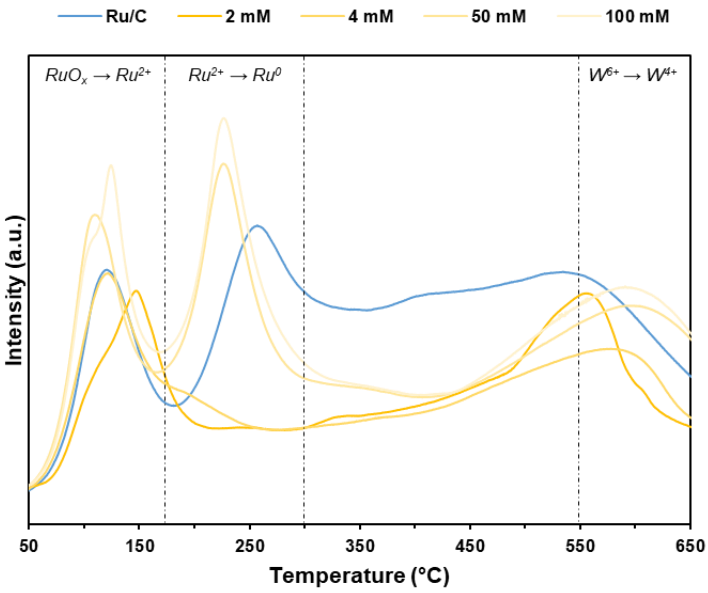


Figure 5. H_2-TPR results of hydrothermally pretreated Ru/C catalysts with $H_4SiW_{12}O_{40}$.

The enhanced C_6 alkane yield observed for Ru/C pretreated with 4 mM $H_4SiW_{12}O_{40}$ suggests that increasing acid incorporation beyond this point does not lead to further improvements. While WO_3 likely boosts activity through increased acidity, excessive acid loading negatively impacts performance. XPS analysis reveals a steady decline in the Ru^0/RuOx ratio with rising $H_4SiW_{12}O_{40}$ concentration – from 0.08 (no HTP) to 0.04 (60 min, 100 mM) – indicating progressive oxidation of Ru^0 (Table 1, Figure S1). This trend is corroborated by TPR, which shows increasing amounts of both RuOx (x > 2) and Ru^{2+} species (Figure 5). The dominant Ru^{2+} signal supports literature reports of a distinct RuO_2 phase forming via interaction between Ru^0 and $H_4SiW_{12}O_{40}$. This modified RuO_2 retains a tetragonal structure but with a reduced c/a ratio, potentially contributing to its lower catalytic activity compared to Ru^0. Characteristic reflections of the modified RuO_2 phase appear at 27.2°, 36°, 38.8°, 53.9°, and 56°.[5,46] For Ru/C catalysts pretreated with higher $H_4SiW_{12}O_{40}$ concentrations (60 min, 50 mM and 100 mM), reflections at 38.8° and 53.9° are clearly observed, suggesting that excess acid promotes formation of this RuO_2 phase (Figure S3b). However, the 53.9° reflection may also correspond to conventional RuO_2, which exhibits a nearby peak at 54.2° (JCPDS 00-040-1290).[31] In contrast, these reflections are absent in catalysts treated with lower acid concentrations (60 min, 2 mM and 4 mM), likely due to either limited interaction with Ru^0 or the formation of amorphous RuO_2 domains to be detected with XRD.

In addition to Ru^0 oxidation, the reduced C_6 alkane yield at high $H_4SiW_{12}O_{40}$ concentrations may also result from restricted access to active Ru sites due to pore blockage or collapse. XPS and TGA analyses show that acid incorporation levels off at higher concentrations (60 min, 50 mM and 100 mM), with minimal differences in W content (1.6 vs. 1.7%) and acid uptake (21 vs. 24%) (Table 1, Figure S1, Table S4), suggesting structural limitations. To explore this, N_2 physisorption was used to assess pore characteristics, revealing a steady decline in meso- and micropore volume, average pore size, and BET surface area with increasing acid concentration – supporting the hypothesis of pore blockage (Table 2). SEM analysis showed no major morphological changes, while XRD confirmed that the graphite structure remained intact across all samples (Figure S7, Figure S3b). According to literature, reflections at 26.6° and 50.2° correspond to the (002) and (102) planes of graphitic carbon, respectively, and are indexed to a hexagonal structure (JCPDS 00-056-0159).[47,48] The (002) reflection at 26.6° was preserved

in all catalysts, though the (102) reflection at 50.2° was only visible in the unpretreated sample, indicating that surface area loss stems from internal pore narrowing rather than structural degradation.

Table 2. TGA and N_2 physisorption results of hydrothermally pretreated Ru/C catalysts.

Entry	Pretreatment		Pore characteristics			
	Time (min)	Acid (mM)	Mesopore volume (cm^3/g)	Micropore volume (cm^3/g)	Average pore size (nm)	BET surface (m^2/g)
1	0	0	0.512	0.175	4.00	735
2	30	0	0.522	0.180	3.95	738
3	60	0	0.530	0.181	3.98	740
4	120	0	0.515	0.180	3.90	723
5	180	0	0.519	0.183	3.94	737
6	60	2	0.456	0.146	3.90	575
7	60	4	0.456	0.146	3.90	575
8	60	50	0.247	0.133	3.36	484
9	60	100	0.230	0.128	3.31	464

Conclusion

Carbon-supported noble metal catalysts show strong promise for the hydrodeoxygenation of carbohydrate-rich streams into naphtha-range alkanes (C_5-C_6), though their performance varies significantly. Ru/C delivered the highest overall alkane yield (79 C%) due to its strong C-O bond cleavage activity, but at the cost of selectivity, promoting unwanted C-C cleavage. Pt/C offered superior C_6 selectivity (56 C%) but is less scalable due to its cost and scarcity. To bridge this gap, Ru/C was modified via HTP in $H_4SiW_{12}O_{40}$ solution, boosting C_6 alkane yield to 56 C% and total naphtha yield to 66 C%, surpassing Pt/C. Mechanistic insights revealed that while longer HTP times increased Ru^0 content, excessive sintering reduced active site availability. Simultaneously, HTP altered the carbon support by reducing surface acidity critical for selective C-O cleavage. Incorporating $H_4SiW_{12}O_{40}$ restored and enhanced weak and medium acidity through WOx formation, though too much acid led to Ru oxidation with loss of catalytic activity, and pore blocking. Thus, carefully tuning HTP conditions is essential to combine Ru's high activity with Pt-like selectivity for efficient, sustainable naphtha production.

Acknowledgements

This work was performed in the framework of the Belgian AD-LIBIO project supported by the Belgian Federal Agency's Energy Transition Fund.

Keywords: Lignocellulosic biomass valorization • Hydrothermal pretreatment • Metal catalyst characterization • Deep catalytic hydrodeoxygenation • Renewable hydrocarbons

[1] S. Dutta, "Sustainable Synthesis of Drop-In Chemicals from Biomass via Chemical Catalysis: Scopes, Challenges, and the Way Forward" *Energy and Fuels* **2023**, *37*, 2648–2666.

[2] T. A. L. Silva, L. H. R. Varão, D. Pasquini in *Handbook of Biomass*, Springer, Singapore, **2024**, pp. 105–142.

[3] Y. Wang, Y. Tian, S. Y. Pan, S. W. Snyder, "Catalytic Processes to Accelerate Decarbonization in a Net-Zero Carbon World" *ChemSusChem* **2022**, *15*, DOI 10.1002/cssc.202201290.

[4] S. Liu, M. Tamura, Y. Nakagawa, K. Tomishige, "One-pot conversion of cellulose into n-hexane over the Ir-ReOx/SiO2 catalyst combined with HZSM-5" *ACS Sustain Chem Eng* **2014**, *2*, 1819–1827.

[5] B. Op De Beeck, M. Dusselier, J. Geboers, J. Holsbeek, E. Morré, S. Oswald, L. Giebeler, B. F. Sels, "Direct catalytic conversion of cellulose to liquid straight-chain alkanes" *Energy Environ Sci* **2015**, *8*, 230–240.

[6] G. W. Huber, R. D. Cortright, J. A. Dumesic, "Renewable alkanes by aqueous-phase reforming of biomass-derived oxygenates" *Angewandte Chemie - International Edition* **2004**, *43*, 1549–1551.

[7] N. Li, G. W. Huber, "Aqueous-phase hydrodeoxygenation of sorbitol with Pt/SiO2-Al2O3: Identification of reaction intermediates" *J Catal* **2010**, *270*, 48–59.

[8] N. Li, G. A. Tompsett, T. Zhang, J. Shi, C. E. Wyman, G. W. Huber, "Renewable gasoline from aqueous phase hydrodeoxygenation of aqueous sugar solutions prepared by hydrolysis of maple wood" *Green Chemistry* **2011**, *13*, 91–101.

[9] Y. T. Kim, J. A. Dumesic, G. W. Huber, "Aqueous-phase hydrodeoxygenation of sorbitol: A comparative study of Pt/Zr phosphate and PtReOx/C" *J Catal* **2013**, *304*, 72–85.

[10] K. Chen, M. Tamura, Z. Yuan, Y. Nakagawa, K. Tomishige, "One-pot conversion of sugar and sugar polyols to n-alkanes without C-C dissociation over the Ir-ReOx/SiO2 catalyst combined with H-ZSM-5" *ChemSusChem* **2013**, *6*, 613–621.

[11] J. Geboers, S. Van De Vyver, K. Carpentier, K. De Blochouse, P. Jacobs, B. Sels, "Efficient catalytic conversion of concentrated cellulose feeds to hexitols with heteropoly acids and Ru on carbon" *Chemical Communications* **2010**, *46*, 3577–3579.

[12] T. Buntara, S. Noel, P. H. Phua, I. Melián-Cabrera, J. G. De Vries, H. J. Heeres, "Caprolactam from renewable resources: Catalytic conversion of 5-hydroxymethylfurfural into caprolactone" *Angewandte Chemie - International Edition* **2011**, *50*, 7083–7087.

[13] Y. Liu, L. Chen, T. Wang, X. Zhang, J. Long, Q. Zhang, L. Ma, "High yield of renewable hexanes by direct hydrolysis-hydrodeoxygenation of cellulose in an aqueous phase catalytic system" *RSC Adv* **2015**, *5*, 11649–11657.

[14] S. Li, L. Jin, H. Wang, X. Wei, W. Li, Q. Liu, X. Zhang, L. Chen, L. Ma, Q. Zhang, "Tungsten oxide decorated silica-supported iridium catalysts combined with HZSM-5 toward the selective conversion of cellulose to C6 alkanes" *Bioresour Technol* **2022**, *347*, 126403.

[15] Q. Bu, H. Lei, A. H. Zacher, L. Wang, S. Ren, J. Liang, Y. Wei, Y. Liu, J. Tang, Q. Zhang, R. Ruan, **2012**, DOI: 10.1016/j.biortech.2012.08.089.

[16] A. Gil, I. Sancho-Sanz, S. A. Korili, **2024**, American Chemical Society preprint, DOI: 10.1021/acs.iecr.4c00747.

[17] A. Carrasco Díaz, L. Abdelouahed, N. Brodu, V. Montes-Jiménez, B. Taouk, **2024**, DOI: 10.3390/molecules29184325.

[18] N. Mussa, K. Toshtay, M. C.- Catalysts, undefined 2024, "Catalytic applications in the production of hydrotreated vegetable oil (HVO) as a renewable fuel: a review" *researchgate.netNS Mussa, K Toshtay, M CapronCatalysts, 2024•researchgate.net* **n.d.**

[19] A. Bjelić, M. Grilc, M. Huš, B. Likozar, "Hydrogenation and hydrodeoxygenation of aromatic lignin monomers over Cu/C, Ni/C, Pd/C, Pt/C, Rh/C and Ru/C catalysts: Mechanisms, reaction micro-kinetic modelling and quantitative structure-activity relationships" *Chemical Engineering Journal* **2019**, *359*, 305–320.

[20] Y. L. Louie, J. Tang, A. M. L. Hell, A. T. Bell, "Kinetics of hydrogenation and hydrogenolysis of 2,5-dimethylfuran over noble metals catalysts under mild conditions" *Appl Catal B* **2017**, *202*, 557–568.

[21] H. Latine, J. Deprez, T. Nicolaï, C. M. Courtin, W. Boerjan, T. Mota, S. Verhelst, T. Robeyn, K. M. Van Geem, O. Mynko, F. H. Vermeire, B. F. Sels, “Catalytic conversion of lignocellulose to naphtha: unlocking sustainable pathways to renewable fuel for engines and feedstock for polymers” *Submitted to Chemical Engineering Journal* **2025**.

[22] T. Komanoya, H. Kobayashi, K. Hara, W. J. Chun, A. Fukuoka, “Catalysis and characterization of carbon-supported ruthenium for cellulose hydrolysis” *Appl Catal A Gen* **2011**, *407*, 188–194.

[23] M. Zhang, J. Chen, H. Li, P. Cai, Y. Li, Z. Wen, “Ru-RuO2/CNT hybrids as high-activity pH-universal electrocatalysts for water splitting within 0.73 V in an asymmetric-electrolyte electrolyzer” *Nano Energy* **2019**, *61*, 576–583.

[24] T. L. Stuchinskaya, M. Musawir, E. F. Kozhevnikova, I. V. Kozhevnikov, “Liquid-phase oxidation of alcohols by oxygen and nitrous oxide catalysed by Ru-Co oxide” *J Catal* **2005**, *231*, 41–47.

[25] T. Komanoya, H. Kobayashi, K. Hara, W. J. Chun, A. Fukuoka, “Catalysis and characterization of carbon-supported ruthenium for cellulose hydrolysis” *Appl Catal A Gen* **2011**, *407*, 188–194.

[26] P. Panagiotopoulou, D. G. Vlachos, “Liquid phase catalytic transfer hydrogenation of furfural over a Ru/C catalyst” *Appl Catal A Gen* **2014**, *480*, 17–24.

[27] A. M. Ruppert, M. Jędrzejczyk, O. Sneka-Płatek, N. Keller, A. S. Dumon, C. Michel, P. Sautet, J. Grams, “Ru catalysts for levulinic acid hydrogenation with formic acid as a hydrogen source” *Green Chemistry* **2016**, *18*, 2014–2028.

[28] M. A. Hossain, T. K. Phung, M. S. Rahaman, S. Tulaphol, J. B. Jasinski, N. Sathitsuksanoh, “Catalytic cleavage of the B-O-4 aryl ether bonds of lignin model compounds by Ru/C catalyst” *Appl Catal A Gen* **2019**, *582*, 117100.

[29] J. Jae, W. Zheng, A. M. Karim, W. Guo, R. F. Lobo, D. G. Vlachos, “The Role of Ru and RuO2 in the Catalytic Transfer Hydrogenation of 5-Hydroxymethylfurfural for the Production of 2,5-Dimethylfuran” *ChemCatChem* **2014**, *6*, 848–856.

[30] X. Lin, Y. Cao, S. Cai, J. Fan, Y. Li, Q. H. Wu, M. Zheng, Q. Dong, “Ruthenium@mesoporous graphene-like carbon: a novel three-dimensional cathode catalyst for lithium–oxygen batteries” *J Mater Chem A Mater* **2016**, *4*, 7788–7794.

[31] C. Boman, J. Danielsen, “Refinement of the crystal structure of ruthenium dioxide” *Acta Chem Scand* **1970**, *24*, 116–122.

[32] L. Sztaberek, H. Mabey, W. Beatrez, C. Lore, A. C. Santulli, C. Koenigsmann, “Sol-Gel Synthesis of Ruthenium Oxide Nanowires to Enhance Methanol Oxidation in Supported Platinum Nanoparticle Catalysts” *ACS Omega* **2019**, *4*, 14226–14233.

[33] L. K. Mcleod, G. H. Spikes, R. J. Kashtiban, M. Walker, A. V. Chadwick, J. D. B. Sharman, R. I. Walton, “Structures of mixed manganese ruthenium oxides (Mn1-xRux)O2 crystallised under acidic hydrothermal conditions” *Dalton Transactions* **2020**, *49*, 2661–2670.

[34] G. Bergeret, P. Gallezot, *Particle Size and Dispersion Measurements*, **2021**.

[35] E. Truszkiewicz, K. Zegadło, D. Wojda, B. Mierzwa, L. Kępiński, “The Effect of the Ruthenium Crystallite Size on the Activity of Ru/Carbon Systems in CO Methanation” *Topics in Catalysis 2017 60:17* **2017**, *60*, 1299–1305.

[36] W. Hu, G. L. Tate, E. Iglesia, “Mechanistic Descriptions and Kinetic Trends in CO2 Hydrogenation on Ru, Co, and Ni Nanoparticles” *ACS Catal* **2025**, *15*, 19503–19516.

[37] V. L. Sushkevich, V. V. Ordomsky, I. I. Ivanova, “Isoprene synthesis from formaldehyde and isobutene over Keggin-type heteropolyacids supported on silica” *Catal Sci Technol* **2016**, *6*, 6354–6364.

[38] M. Almohalla, I. Rodríguez-Ramos, A. Guerrero-Ruiz, “Comparative study of three heteropolyacids supported on carbon materials as catalysts for ethylene production from bioethanol” *Catal Sci Technol* **2017**, *7*, 1892–1901.

[39] S. S. Wang, X. Chen, Y. Tan, Z. Zhao, W. Yang, C. Huang, X. Wang, M. M. Chen, Z. Du, Y. Ding, “Highly efficient synthesis of isoprene from methyl tert-butyl ether and formaldehyde over activated carbon supported silicotungstic acid catalysts” *Molecular Catalysis* **2020**, *485*, 110840.

[40] T. Kim, R. S. Assary, C. L. Marshall, D. J. Gosztola, L. A. Curtiss, P. C. Stair, “Acid-catalyzed furfuryl alcohol polymerization: Characterizations of molecular structure and thermodynamic properties” *ChemCatChem* **2011**, *3*, 1451–1458.

[41] R. Kloth, D. V. Vasilyev, K. J. J. Mayrhofer, I. Katsounaros, “Electroreductive 5-Hydroxymethylfurfural Dimerization on Carbon Electrodes” *ChemSusChem* **2021**, *14*, 5245–5253.

[42] A. G. Scroggie, G. L. Clark, “THE CRYSTAL STRUCTURE OF ANHYDROUS SILICOTUNGSTIC ACID 1 AND RELATED COMPOUNDS AND THEIR PROBABLE MOLECULAR FORMULAS” *Proceedings of the National Academy of Sciences* **1929**, *15*, 1–8.

[43] I. V. Kozhevnikov, A. Sinnema, R. J. J. Jansen, H. van Bekkum, “17O NMR determination of proton sites in solid heteropoly acid H3PW12O40.31P,29Si and17O NMR, FT-IR and XRD study of H3PW12O40 and H4SiW12O40 supported on carbon” *Catal Letters* **1994**, *27*, 187–197.

[44] L. R. Pizzio, C. V. Cáceres, M. N. Blanco, “Adsorption of tungstophosphoric or tungstosilicic acids from ethanol-water solutions on carbon” *J Colloid Interface Sci* **1997**, *190*, 318–326.

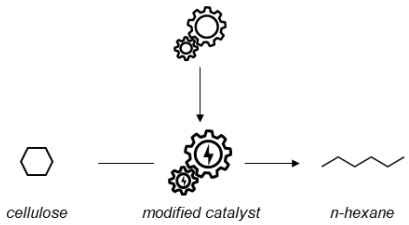
[45] M. Weil, W. Schubert, “The beautiful colours of tungsten oxides” *Materials Science* **2013**.

[46] M. L. Foo, Q. Huang, J. W. Lynn, W. L. Lee, T. Klimczuk, I. S. Hagemann, N. P. Ong, R. J. Cava, “Synthesis, structure and physical properties of Ru ferrites: BaMRu 5O11 (M=Li and Cu) and BaM′2Ru 4O11 (M′=Mn, Fe and Co)” *J Solid State Chem* **2006**, *179*, 563–572.

[47] Q. T. Ain, S. H. Haq, A. Alshammari, M. A. Al-Mutlaq, M. N. Anjum, “The systemic effect of PEG-nGO-induced oxidative stress in vivo in a rodent model” *Beilstein Journal of Nanotechnology* **2019**, *10*, 901–911.

[48] L. Alcaraz, C. Díaz-Guerra, J. Calbet, M. L. López, F. A. López, “Obtaining and Characterization of Highly Crystalline Recycled Graphites from Different Types of Spent Batteries” *Materials* **2022**, *15*, DOI 10.3390/ma15093246.

Entry for the Table of Contents



This work demonstrates that controlled hydrothermal pretreatments make Ru/C highly selective for converting carbohydrate waste into naphtha-range alkanes. By tuning acidity, oxidation state, and porosity, we boost selectivity while keeping higher activity and lower cost compared to other noble metals, enabling a scalable pathway towards renewable fuels and polymer precursors.